Biomass burning smoke aerosol properties measured during Fire Laboratory at Missoula Experiments (FLAME)

E. J. T. Levin,[1] G. R. McMeeking,[1,2] C. M. Carrico,[1] L. E. Mack,[1] S. M. Kreidenweis,[1] C. E. Wold,[3] H. Moosmüller,[4] W. P. Arnott,[4] W. M. Hao,[3] J. L. Collett Jr.,[1] and W. C. Malm[5]

Received 24 November 2009; revised 18 May 2010; accepted 8 June 2010; published 25 September 2010.

[1] During the Fire Laboratory at Missoula Experiments (FLAME), we studied the physical, chemical, and optical properties of biomass burning smoke from the laboratory combustion of various wildland fuels. A good understanding of these properties is important in determining the radiative effects of biomass burning aerosols, with impacts on both local and regional visibility and global climate. We measured aerosol size distributions with two instruments: a differential mobility particle sizer (DMPS) and an optical particle counter (OPC). Volume size distributions from different burns varied from monomodal to multimodal, with geometric mean diameters ranging from 0.20–0.57 μm and geometric standard deviations ranging from 1.68–2.97. By reconciling the differences between the two sizing instruments, we estimated aerosol effective refractive indices with values ranging from 1.41 to 1.61. We reconstructed aerosol chemical composition for each burn using data from filters collected and analyzed with the Interagency Monitoring of Protected Visual Environments (IMPROVE) samplers and protocols. Aerosols were generally comprised of carbon with organic species accounting for the largest mass fraction in most cases. We used composition data to calculate aerosol density, which ranged from 1.22–1.92 g cm^{-3}, and real and imaginary refractive indices, which had ranges of 1.55–1.80 and 0.01–0.50 respectively. Aerosol physical, chemical, and optical characterizations were combined to calculate dry mass scattering (MSE) and absorption (MAE) efficiencies at 532 nm. These parameters had values between 1.6–5.7 m^2 g^{-1} and 0.04–0.94 m^2 g^{-1}.

Citation: Levin, E. J. T., et al. (2010), Biomass burning smoke aerosol properties measured during Fire Laboratory at Missoula Experiments (FLAME), *J. Geophys. Res.*, *115*, D18210, doi:10.1029/2009JD013601.

1. Introduction

[2] Biomass burning, from both prescribed burning and wildfires, is one of the largest contributors to global accumulation mode aerosol mass [*Chen et al.*, 2007; *Kasischke and Penner*, 2004]. These emissions not only greatly increase local aerosol mass concentrations but can also be transported over long distances, leading to regionally elevated aerosol loadings [*McMeeking et al.*, 2006]. Smoke particles are a major source of both elemental (EC) and organic (OC) carbonaceous particulate matter, especially in the western and southeastern United States [*Park et al.*, 2007]. Elemental carbon strongly absorbs light at visible and UV wavelengths and both EC and OC aerosols scatter visible light [*Reid et al.*, 2005a]. Because of their global distributions, high concentrations, and radiative properties, these emissions have a large impact on both global radiation budgets and local visibility reduction.

[3] Visibility reduction is one of the most obvious manifestations of air pollution and, thus, there are federal mandates requiring visibility protection and improvement in protected areas. In 1977, Congress amended the 1970 Clean Air Act setting forth as a national goal the improvement of visibility in federally mandated Class I areas (national parks and wilderness areas) as well as the prevention of future visibility degradation in these areas [*Watson*, 2002]. In 1988 the Interagency Monitoring of Protected Visual Environments (IMPROVE) network was established to measure visibility in Class I areas as well as the pollutants responsible for visibility reduction [*Malm et al.*, 1994]. Improving visibility in Class I areas was given even greater importance in 1999 with the passing of the Regional Haze Rule (RHR). The RHR requires that visibility in federally protected areas must be returned to natural levels within 60 years [*Watson*, 2002].

[1]Department of Atmospheric Science, Colorado State University, Fort Collins, Colorado, USA.
[2]Now at the Centre for Atmospheric Science, University of Manchester, Manchester, U. K.
[3]Fire Sciences Laboratory, Rocky Mountain Research Station, USDA Forest Service, Missoula, Montana, USA.
[4]Division of Atmospheric Sciences, Desert Research Institute, Reno, Nevada, USA.
[5]U.S. National Park Service, Cooperative Institute for Research in the Atmosphere, Colorado State University, Fort Collins, Colorado, USA.

0148-0227/10/2009JD013601

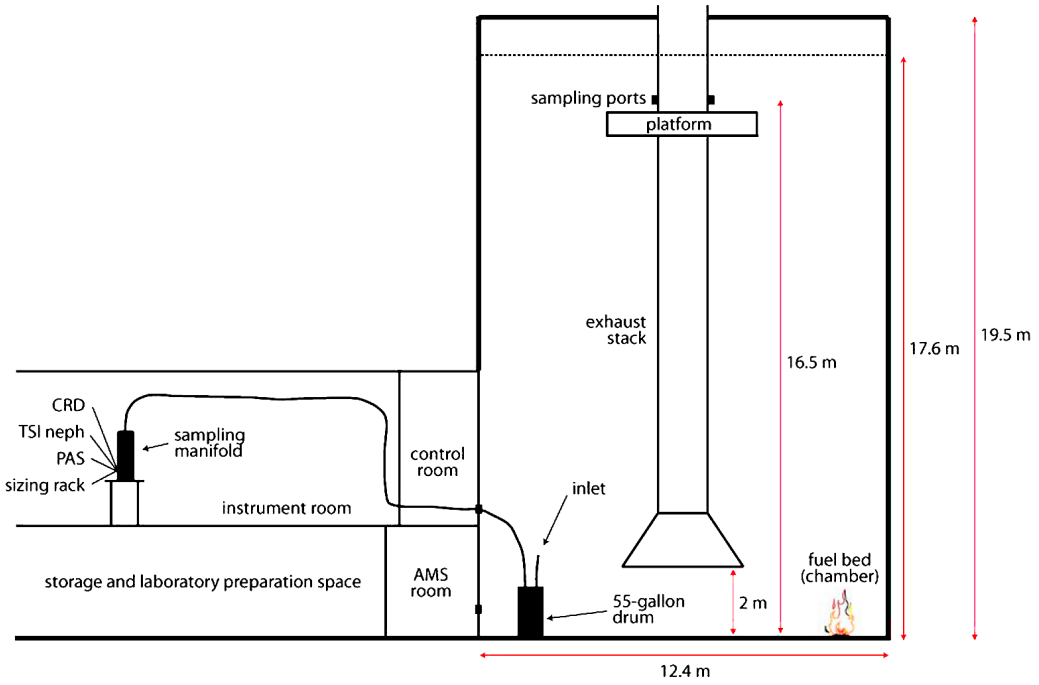

Figure 1. Diagram of the FSL combustion facility (modified from *McMeeking et al.* [2009]).

[4] In order to reach the goals set forth by the RHR and to understand the role of smoke particles in the global radiation budget, characterization of the optical behavior of biomass burning aerosols, dependent on both physical and chemical properties, is necessary. For example, mass scattering efficiencies are used in global models to calculate the radiative effects of aerosols and are also used to calculate light extinction from mass concentrations measured in monitoring networks to determine compliance with the RHR [*Hand and Malm*, 2007; *Pitchford et al.*, 2007]. Global and regional models also utilize complex refractive indices (often calculated from some assumed OC/EC split) and Mie theory to calculate aerosol radiative effects [*Bäumer et al.*, 2007].

[5] Many previous field studies have examined the gaseous and particulate-phase emissions from wild fires and prescribed burning [*Abel et al.*, 2003; *Andreae et al.*, 1998; *Christian et al.*, 2007; *Formenti et al.*, 2003; *Hodzic et al.*, 2007; *Yokelson et al.*, 2009]. While these field campaigns greatly increased our understanding of biomass burning emissions, these measurements are typically made downwind of the source, the measured smoke is likely from a mixture of various vegetation types, and the sample may be mixed with non-biomass burning aerosols. These measurements must also account for a wide range in fire and meteorological variables [*Reid et al.*, 2005b]. For example, *McMeeking et al.* [2005a, 2005b] calculated the refractive index of smoke-impacted aerosols at Yosemite National Park, but their measurements included other non-biomass burning emissions as well as non-quantifiable aging processes. Laboratory burn experiments, however, allow for measurement of fire-integrated smoke properties from a single fuel type under relatively controlled conditions. We are also able to measure dry aerosol properties in the lab, whereas ambient smoke particles, depending on the environmental relative humidity, can have small to substantial water contents.

2. Methods

[6] The Fire Laboratory at Missoula Experiments (FLAME 1 and 2) were conducted during May and June of 2006 and 2007 at the United Sates Forest Service's (USFS) Fire Sciences Lab (FSL) in Missoula, Montana. During both FLAME studies, selected wildland fuels were burned in a controlled laboratory environment to examine the effects of fuel type, fuel moisture, fire behavior, fuel amount, and other related variables on gas and particle emissions. We measured aerosol physical, chemical, and optical properties and concentrations of gaseous species emitted from the fire with both real time and filter-based instrumentation. An overview of fuels burned, many of the measurements and some initial results are available from *McMeeking et al.* [2009], *Petters et al.* [2009a, 2009b], *Carrico et al.* [2010], and *Mack et al.* [2010]. Here, we present aerosol chemical data from FLAME 1 and 2 as well as aerosol physical data from FLAME 2. We also use FLAME 2 data to calculate mass scattering and absorbing efficiencies.

2.1. Experimental Setup

[7] The biomass burning experiments performed during FLAME were conducted in a 3000 m^3 burn chamber at the FSL (Figure 1). For each experiment, between 50 and 250 g of fuel were placed on a ceramic fuel bed and ignited with a propane torch (primarily used during FLAME 1) or an electrical heating coil, using ~10 ml of ethanol as an accelerant, (used for all FLAME 2 burns). The heating coil ignition system caused the entire fuel bed to ignite simultaneously

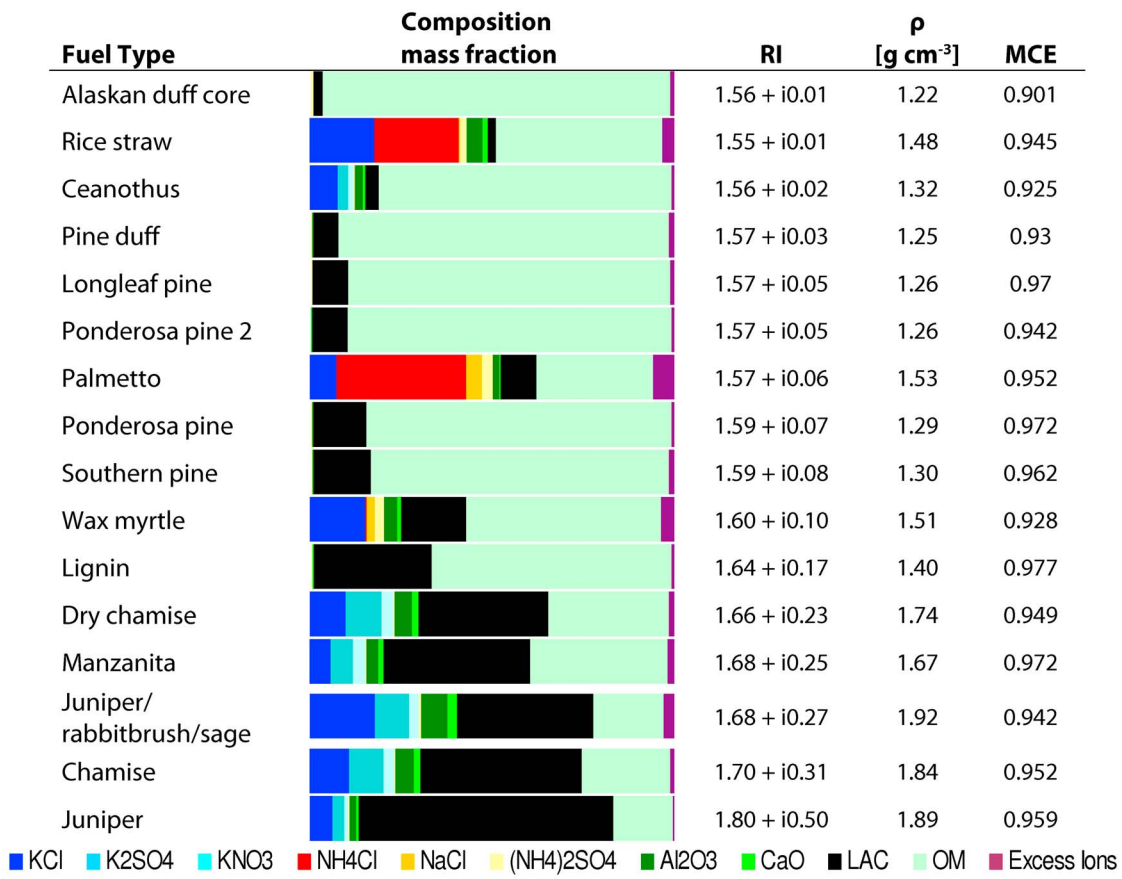

Figure 2. $PM_{2.5}$ aerosol composition for each FLAME 1 chamber burn as well as calculated refractive indices and densities from IMPROVE data and burn integrated modified combustion efficiency. Burns are ranked from least to most light absorbing.

while the propane torch created a flame front which propagated through the fuel.

[8] We present results from a subset of the FLAME experiments, chamber burns, in which the burn chamber was sealed and smoke was allowed to fill the entire room. Because of the small amount of fuel used for each experiment, the fires typically lasted 5–15 min; however, the smoke was held in the chamber for one to several hours. Although this variation in experiment length affected aerosol concentrations and size distributions (discussed below), optical properties such as single scattering albedo calculated from continuous measurements [*Mack et al.*, 2010] and retrieved effective refractive indices (discussed below) remained nearly constant over the course of every experiment.

[9] The fuels burned (Figures 2 and 3) were chosen to represent the plant species frequently burned in the western and southeastern regions of the United States, as well as Asian rice straw and sugarcane, commonly burned agricultural byproducts. Replicate experiments were performed with ponderosa pine during FLAME 1 and black needlerush, Alaskan duff core and dry Douglas fir during FLAME 2. In these cases the second burn is denoted by a 2. Several fuels, such as rice straw, longleaf pine, chamise and Alaskan duff, were burned during both FLAME studies. The dry chamise and dry Douglas fir fuels were preconditioned by being stored for 48 h in a climate controlled room kept at 35–40°C. All other fuels were burned with no previous treatment other than drying that occurred naturally during shipping and storage.

[10] The fire-integrated modified combustion efficiency (MCE) for each burn, as determined by *McMeeking et al.* [2009], is also indicated in Figures 2 and 3. The MCE qualitatively indicates whether the emissions were primarily produced during smoldering or flaming combustion and is important to consider because the properties of emitted particles are expected to depend strongly on combustion phase.

2.2. Instrumentation

[11] During both FLAME studies, two IMPROVE samplers [*DeBell et al.*, 2006] located in the burn chamber collected $PM_{2.5}$ and PM_{10} aerosols for subsequent compositional analysis. The typical IMPROVE sampler configuration described by *DeBell et al.* [2006] was modified such that both $PM_{2.5}$ and PM_{10} samples were collected onto Teflon, nylon and quartz filters. The nylon filters were analyzed via ion chromatography for NO_3^-, SO_4^{2-}, Cl^-, NH_4^+, Na^+ and K^+, a wider array of ions than is typically analyzed as part of the IMPROVE network protocol. The Teflon filters were weighed before and after sampling to determine total gravi-

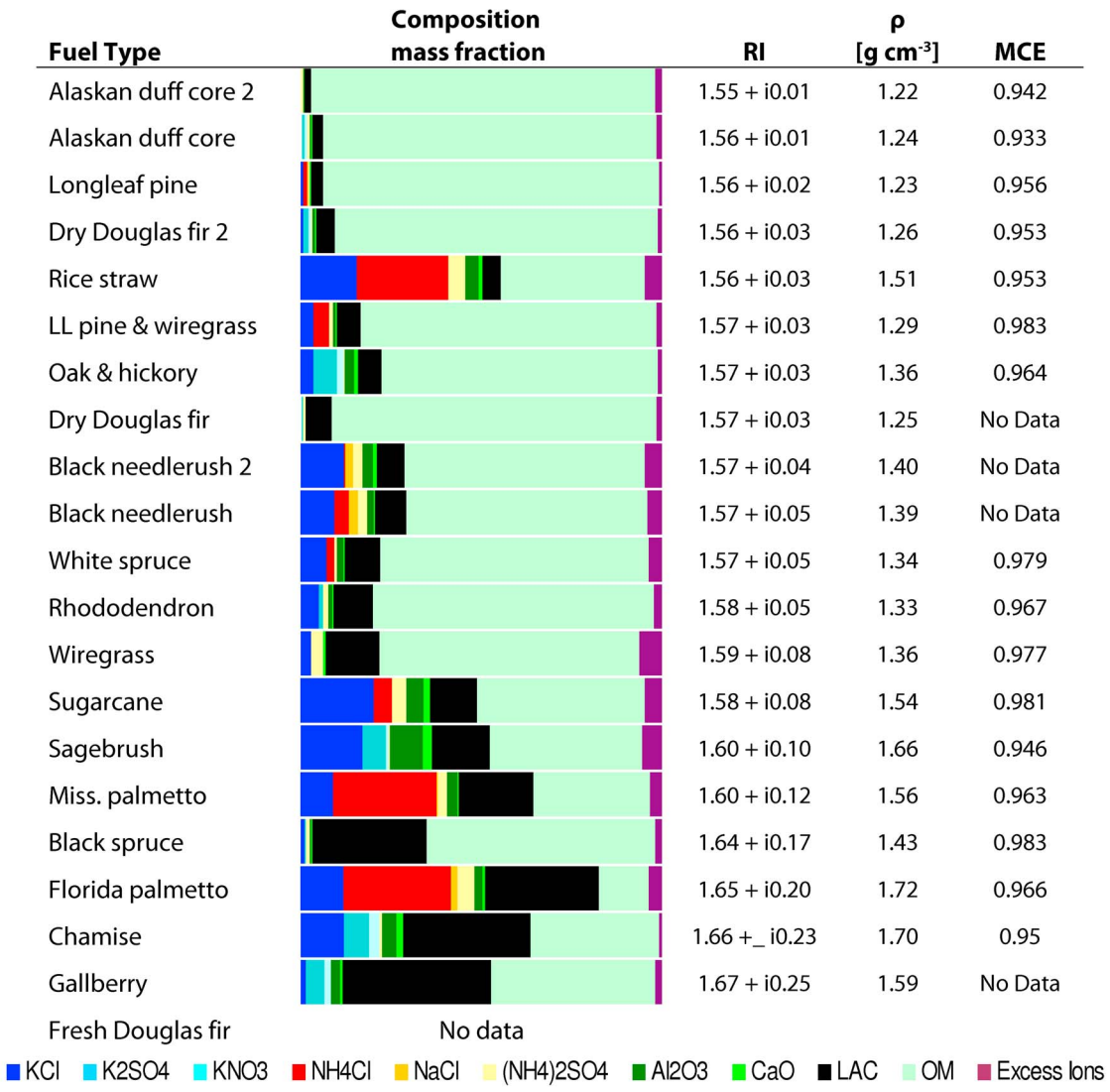

Figure 3. $PM_{2.5}$ aerosol composition for each FLAME 2 chamber burn as well as calculated refractive indices and densities from IMPROVE data and burn integrated modified combustion efficiency. Burns are ranked from least to most light absorbing.

metric mass loading and were then used to determine concentrations of the elements Al, Si, Ca, K, Fe, Ti, Mg and Na via X-ray fluorescence analysis. The quartz filters were used to determine concentrations of carbonaceous aerosols via Thermal Optical Reflectance (TOR) analysis following the IMPROVE_A protocol [*Chow et al.*, 2007]. Separate filter sets were collected for each burn. Further details regarding the chemical sampling and analyses are provided in *McMeeking et al.* [2009].

[12] During FLAME 2, aerosols were also collected by additional high volume filter samplers located on the burn chamber floor. These filters were subsequently analyzed in the laboratory at Colorado State University using a Sunset Laboratory (Forest Grove, Oregon) carbon analyzer following the NIOSH 5040 protocol [*Bae et al.*, 2004] to determine OC and EC concentrations.

[13] During FLAME 2, two instruments, a differential mobility particle sizer (DMPS; TSI 3081 differential mobility analyzer with TSI 3785 water-based condensation particle counter) and an optical particle counter (OPC; PMS LASAIR 1003), measured aerosol number size distributions with 10 min temporal resolution over the diameter ranges 0.04–0.63 μm and 0.2–2.0 μm respectively. Instrument calibrations were checked twice during the FLAME 2 study with polystyrene latex (PSL) spheres of known sizes. Both instruments sized the test particles into the correct bins in every case.

[14] The DMPS was operated at a sample flow rate of 0.3 LPM and a sheath flow rate of 3.0 LPM. The OPC sampled at 0.028 LPM to reduce the possibility of particle coincidence in the detection region. At these conditions, the manufacturer reports an upper concentration limit of

13 000 cm^{-3}. The probability of coincidence errors greatly increases for concentrations above these levels, thus the OPC data cannot be used in these cases [*Hand and Kreidenweis*, 2002]. Even with the small amounts of fuel burned and the large mixing volume in the burn chamber, aerosol concentrations often exceeded the OPC saturation limit. For those times, we used only DMPS data to construct aerosol size distributions and did not determine the aerosol refractive index from size distribution analysis.

[15] Sample flow for the sizing instruments was drawn into a 55 gallon drum in the burn chamber and then through a 1 inch diameter stainless steel tube from the drum to a smaller sampling manifold in the adjacent instrument room (Figure 1). The two sizing instruments drew the sample from a common manifold outlet at a flow of 0.6 LPM which was split isokinetically into two 0.3 LPM flows. Because the OPC only required a sample flow of 0.028 LPM, the excess flow was siphoned off prior to the OPC inlet using a critical orifice. Although the sample for the sizing instruments was not actively dried, because the relative humidity in the burn chamber was very low, typically less than 20%, we treat the measurements as dry in this analysis. Aerosol losses in the sampling lines between the manifold and the sizing instruments were calculated following *Hand* [2001] and the data were adjusted accordingly.

[16] A photoacoustic spectrometer (PAS), built and operated by the University of Nevada's Desert Research Institute (DRI), sampled from the same manifold as the sizing instruments. This instrument measured aerosol light absorption at 532 nm and is described in greater detail by *Arnott et al.* [1999] and *Moosmüller et al.* [2009]. *Arnott et al.* [2000] describe a calibration method for the PAS which was performed before FLAME 2.

[17] A TSI 3563 nephelometer, which also sampled from the common manifold, measured aerosol light scattering coefficients at 450, 550 and 700 nm. Scattering coefficients at 532 nm were interpolated using the three measured values [*Mack*, 2008]. The instrument detects scattering over the range of angles 7–170° [*Anderson et al.*, 1996], thus light scattered primarily in the forward or backward direction is not detected [*Moosmüller and Arnott*, 2003]. Truncation and non-Lambertian light source errors were corrected following *Anderson and Ogren* [1998], although *Bond et al.* [2009] have shown that this correction is in error from 1 to 5% if absorbing particles are present, as is the case for some biomass burning aerosol. The TSI nephelometer was calibrated with filtered air, CO_2, and SUVA (HFC 134a) at the end of FLAME 2.

2.3. Alignment Method

[18] The OPC detects light scattered by a particle passing through a laser beam (632.8 nm) and uses the magnitude of this signal to size the particle into one of eight PSL-calibrated bins. Because light scattering is a function of the particle's refractive index, the OPC response is also affected by this parameter. That is, the OPC may size particles with the same physical diameter (assuming spherical particles) but different refractive indices into different bins. The OPC, therefore, reports an optical diameter. We exploit the dependence on refractive index to fit the OPC output to that of the DMPS following the alignment procedure developed by *Hand and Kreidenweis* [2002]. The alignment method has been used previously to examine the optical properties of ambient aerosols sampled in several national parks [*Hand et al.*, 2002; *Levin et al.*, 2009; *McMeeking et al.*, 2005a, 2005b].

[19] Prior to FLAME 2, we characterized the OPC response to different real refractive indices (n) using DMA mobility size selected ammonium sulfate (n = 1.53) and oleic acid (n = 1.46) particles. These data, as well as the manufacturer's PSL (n = 1.588) calibration points, were used to construct OPC response curves for each bin as functions of n. We applied these OPC response curves to adjust the OPC bin limits for any assumed refractive indices between 1.40 and 1.70. The alignment code scans through this n range in increments of 0.005, adjusts the OPC bin limits at each value and calculates dry volume distributions from the adjusted number distributions. The code then compares this new volume distribution with that calculated from the DMPS in the overlap region between the two instruments by fitting a zero-intercept linear regression to the data; volume distributions were used to align the DMPS and OPC because they are more sensitive in the overlap region between the two instruments [Hand, 2001]. If the two volume distributions agree perfectly, the slope of this line will be 1. Following *Hand* [2001], a successful alignment was defined as those cases where the best fit regression line slope was between 0.8 and 1.2. The agreement between the two volume distributions is determined by calculating the χ^2 goodness-of-fit between the aligned data and a 1:1 line. The n value resulting in the minimum χ^2 is assumed to be the effective refractive index (m) of the aerosol population. The final step of the alignment process is to average together the best fit OPC and DMPS distributions to obtain a single volume size distribution for each 10 min sample. We then generated aligned number size distributions from the aligned volume distributions. As described in the auxiliary material, we also adjusted the OPC volume distributions for the refractive indices calculated from aerosol chemical composition (section 4) and compared these to the DMPS distribution as described above.[1]

[20] Although we can only determine the OPC's response to purely scattering particles, the effective refractive index determined from the above method is a function of both the real (n) and imaginary (k) parts of the aerosol's refractive index. Thus, we denote it with m. If a particle is highly light absorbing, the OPC resolution is degraded for physical diameters larger than about 0.3 μm. As shown by *Hand and Kreidenweis* [2002], absorbing particles with physical diameters between about 0.3 to 1.0 μm have similar optical diameters and are thus sized into one bin, with the exact response depending on how strongly absorbing they are. Generally, the bins for PSL particles >0.3 μm are not assigned any counts for such particles. In the alignment procedure, the OPC volume distributions, computed as functions of n, move toward smaller diameters as n increases [*Hand and Kreidenweis*, 2002]. For highly absorbing aerosols, in order to compensate for undercounting of particles larger than 0.3 μm diameter in the OPC volume distributions as compared with the volume distributions from the DMPS, the minimum χ^2 will occur at lower n values, which shift the

[1] Auxiliary materials are available in the HTML. doi:10.1029/2009JD013601.

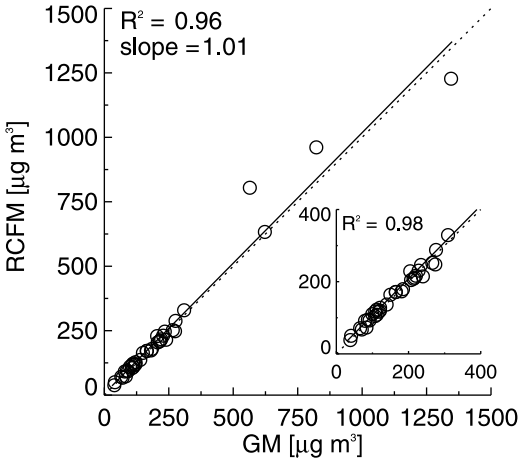

Figure 4. Reconstructed $PM_{2.5}$ mass concentration [$\mu g\ m^{-3}$] versus $PM_{2.5}$ gravimetric mass concentration [$\mu g\ m^{-3}$]. Solid line is the regression line; dotted line is the 1:1 line.

OPC distribution toward larger diameters. Therefore, the retrieved effective refractive index will be lower than the true real part of the refractive index for absorbing particles. This discrepancy between the actual complex and retrieved effective refractive indices is expected to increase as absorption increases.

[21] Another source of uncertainty in the sizing data is particle shape. Soot aggregates can form highly non-spherical chain aggregates which affect sizing by the DMA and OPC through changes in aerodynamic and optical properties [*Chakrabarty et al.*, 2006; *DeCarlo et al.*, 2004; *Liu et al.*, 2008; *Slowik et al.*, 2004]. The shape and morphology of fresh carbonaceous aerosols from biomass burning depend on many factors especially combustion temperature [*Bond and Bergstrom*, 2006]. However, even highly non-spherical particles typically compact and become more spherical with time [*Chakrabarty et al.*, 2007]. *Martins et al.* [1998] reported that after just one hour of atmospheric aging, most biomass burning aerosols can be considered spherical, and thus Mie theory is applicable. *Mack et al.* [2010] examine the effects of aerosol shape factor on optical properties measured during FLAME 2. The data reported here are not corrected for these possible shape effects.

3. Aerosol Composition

[22] Aerosol $PM_{2.5}$ composition for each of the FLAME 1 and 2 chamber burns was reconstructed using filter data from the IMPROVE samplers. Reconstructed fine mass (RCFM) concentration was calculated as

$$[\mathrm{RCFM}] = [\mathrm{SALTS}] + [\mathrm{DUST}] + [\mathrm{OM}] + [\mathrm{LAC}] \qquad (1)$$

where the terms on the right hand side are the mass concentrations of inorganic salts, elemental crustal material, organic species and light absorbing carbon respectively. Each of these components was calculated as follows.

[23] To calculate the mass concentration of inorganic salts (SALTS), we first assumed that K^+ and Cl, the two most abundant ions for most burns, were in the form of KCl^-, and NH_4^+ and SO_4^{2-}, the next most abundant species, were in the form of $(NH_4)_2SO_4$. Any remaining K^+ was apportioned to K_2SO_4 or KNO_3, based on the abundance of the other ions, and any excess Cl^- was likewise apportioned to NH_4Cl and NaCl. These potassium salts are commonly found in biomass burning plumes [*Freney et al.*, 2009]. Using the above assumptions, almost all of the measured inorganic ions were accounted for in every burn. We grouped any remaining ions into "excess ions" and included their mass explicitly in SALTS. The excess ions accounted for less than 6% of the total aerosol mass for every experiment.

[24] Most of the burns produced aerosols with small amounts of Al and Ca, as determined by XRF analysis. These elements were assumed to be present as Al_2O_3 and CaO, and we included the mass concentrations of these species in the RCFM as DUST, following the IMPROVE convention [*Pitchford et al.*, 2007].

[25] The mass concentration of organics was calculated by multiplying the mass concentration of OC, determined from TOR analysis, by a coefficient to account for other elements, such as H, O and N, that contribute to organic mass (OM). The IMPROVE network uses a value of 1.8 for this coefficient [*Pitchford et al.*, 2007]. However, because of the wide range of organic molecules, there is likewise a wide range in possible values for this coefficient [*Malm and Hand*, 2007; *Turpin and Lim*, 2001]. We found that a value of 1.55 gave the best overall agreement between measured gravimetric mass (GM) concentration and RCFM. This value is in good agreement with the findings of *Reid et al.* [2005b], who reported an OM/OC mass ratio ~1.5 for biomass burning emissions. The mass concentration of light absorbing carbon (LAC) was assumed to be equal to that of elemental carbon reported from the TOR analysis.

[26] There are, of course, other sets of assumptions which could be employed to reconstruct aerosol mass. However, we believe the above speciation is reasonable, and, as can be seen in Figure 4, using the above assumptions, RCFM compares very well with measured GM ($R^2 = 0.96$ and slope = 1.01). There are still small discrepancies between GM and RCFM which could be completely reconciled by adjusting the OC multiplier for each burn. However, the 1.55 value provides good closure within the uncertainties inherent in the filter sampling and analysis techniques and the assumptions involved in mass reconstruction. For all of the FLAME data, the reported average and one standard deviation percent uncertainty in $PM_{2.5}$ GM was 45 ± 16%. The reported uncertainties for each of the measured $PM_{2.5}$ mass components, however, were much smaller. Propagating these uncertainties through the RCFM calculations gave an average and one standard deviation percent uncertainty of only 3.1 ± 1%.

[27] On average, $PM_{2.5}$ accounted for 85% of total PM_{10} mass. Both measured OC and EC PM_{10} mass were about 90% accounted for by $PM_{2.5}$ while close to 100% of the inorganic ions were in the $PM_{2.5}$ fraction. Only DUST had higher mass concentrations above 2.5 μm, with an average $PM_{2.5}$ to PM_{10} ratio of 0.46 over all burns.

[28] Aerosol $PM_{2.5}$ composition for almost every burn (Figure 2 for FLAME 1 and Figure 3 for FLAME 2) was highly carbon dominated with OM accounting for the largest mass fraction in most cases. During FLAME 1 several burns, those involving chamise, manzanita, and juniper fuels, had larger mass fractions of LAC than OM. During FLAME 2,

Table 1. Densities and Refractive Indices for Species Used in Reconstructed Fine Mass Calculations

Species	Density (g cm^{-3})	Refractive Index
KCl	1.99[a]	1.49[a]
K_2SO_4	2.66[a]	1.50[a]
KNO_3	2.11[a]	1.50[a]
NH_4Cl	1.53[a]	1.55[a]
NaCl	2.16[a]	1.54[a]
$(NH_4)_2SO_4$	1.76[b]	1.53[b]
Al_2O_3	3.97[a]	1.77[a]
CaO	3.30[a]	1.83[a]
Organic Carbon	1.20[c]	1.55[d]
Light Absorbing Carbon	1.70–2.1[e]	1.75−.63i–1.95−.79i[e]

[a]*Lide* [2008].
[b]*Tang* [1996].
[c]*Turpin and Lim* [2001].
[d]*Hand and Kreidenweis* [2002].
[e]*Bond and Bergstrom* [2006].

only the Florida palmetto burn produced aerosols with a higher mass fraction of LAC than OM, although the two fractions were similar for the gallberry and chamise burns. The Mississippi palmetto and black spruce burns also produced large quantities of LAC; however, in both cases the OM fraction was still larger. The rice straw and palmetto burns during both FLAME studies produced mass fractions of SALTS close to 0.5. The FLAME 2 sagebrush burn and the FLAME 1 mixed juniper/rabbitbrush/sage burn had the highest DUST mass fractions, close to 0.1.

[29] The particles from fuels burned in replicate experiments, both those repeated during the same study and those burned during both FLAME studies, all showed similar composition profiles. Note that the palmettos were not included in this comparison because of the differences in the fuel's location of origin. For every duplicate fuel, except chamise, the mass fractions of each component were within 5% or less. In the case of the two chamise experiments, one performed during FLAME 1 and the other during FLAME 2, the difference in OM mass fractions was 11% and that of LAC 8%. The difference in total carbon mass fractions, however, was only 3%. This difference in carbon apportionment could be due to fire intensity, possibly a result of fuel moisture or the differences in ignition technique between FLAME 1 and 2.

4. Aerosol Properties Calculated From Composition

[30] Dry aerosol complex refractive index (m) and density (ρ) were calculated from the composition data presented above, assuming the particles are all internally mixed, and using [*Hasan and Dzubay*, 1983]

$$\overline{\rho}^{-1} = \sum_i \frac{X_i}{\rho_i} \tag{2}$$

$$m = \overline{\rho} \sum_i \frac{X_i n_{i,i}}{\rho_i} - \overline{\rho} \sum_i \frac{X_i k_i}{\rho_i} i \tag{3}$$

where X_i is the mass fraction of each component and ρ_i, n_i and k_i are the density and real and imaginary refractive indices for each component (Table 1). The densities and complex refractive indices calculated for each burn are listed in Figures 2 and 3. These values use the higher LAC values listed in Table 1 (discussed below). Because we do not know what salts are formed by the excess ions, they were not included in the above calculations. However, we found that including them, using various assumed representative ρ_i and n_i values, changed the results by less than 1% in all cases. We assume that our chemically derived refractive index values are valid across visible wavelengths [*Bond and Bergstrom*, 2006; *Lide*, 2008].

[31] Across both FLAME 1 and 2 burns, aerosol density calculated from composition (ρ_{comp}) varied from 1.22–1.92 g cm^{-3} with the FLAME 1 Alaskan duff core and the FLAME 2 Alaskan duff core 2 burns producing the lowest density aerosol and the mixed juniper/rabbitbrush/sage burn the highest. Across both FLAME studies, real refractive index (n_{comp}) values ranged from 1.55–1.80 and imaginary (k_{comp}) values from 0.01–0.50. The FLAME 2 Alaskan duff core 2 burn produced aerosols with the lowest values of both n_{comp} and k_{comp} while the juniper burn produced aerosols with the highest. The correlation between the real and imaginary parts of the refractive index in these composition based calculations is due to the fact that the refractive index value we are using for LAC has the highest value of n, and is the only component with a nonzero value of k. Thus, the magnitude of both n_{comp} and k_{comp} is an indicator of the mass fraction of LAC. The burns in Figures 2 and 3 are ranked from least to most absorbing, that is from lowest to highest k_{comp}.

[32] Because LAC plays such an important role in determining the refractive indices calculated from composition, it is important to accurately know both the mass fraction of LAC and the refractive index of this component. There are, however, considerable uncertainties in both of these parameters. The measured split between organic and elemental carbon depends on analysis technique [*Watson et al.*, 2005]. Thermal optical analysis (TOA) methods for analyzing carbon heat a filter punch first in an oxygen free environment, which causes OC to volatilize, and then add oxygen to combust EC. Concentrations of OC and EC are determined by analyzing the evolved carbon gases during the two phases. The split between OC and EC, however, is not always clearly defined as some of the organic carbon can pyrolyze during the first, oxygen free, stage and then evolve during the second stage. Although pyrolized carbon is corrected for in the IMPROVE_A analysis, this still introduces some uncertainty into the OC/EC split [*Chow et al.*, 2007]. The split between measured OC and EC also depends on the level of heating during the two stages of analysis which vary according to different measurement protocols. Several investigators have also reported that the presence of K^+ and Na^+, which are often found in biomass burning aerosol, can also effect the OC/EC split by decreasing the combustion temperature for EC [*Boparai et al.*, 2008; *Novakov and Corrigan*, 1995]. Because of these factors, two different carbon analysis instruments generally give different values of OC and EC concentrations even from the same filter samples [*Watson et al.*, 2005].

[33] For the FLAME 2 samples, total carbon determined by the IMPROVE and Sunset analysis techniques agreed well for each burn. However, the Sunset analyzer generally apportioned more carbon to OC than EC [*McMeeking et al.*, 2009]. The effect of this different OC/EC split will be discussed below.

Table 2. Geometric Mean and Standard Deviations for Number and Volume Size Distributions As Well As Retrieved Effective Refractive Indices and Best Fit Alignment Parameters for FLAME 2 Burns

Fuel	D_{gn} (μm)		σ_{gn}		D_{gv} (μm)		σ_{gv}		V Distribution Modes	$m_{retrieved}$ Average	N	χ^2 Average	Slope Average
	Initial	1 h	Initial	1 h	Initial	1 h	Initial	1 h					
Alaskan duff core 2	0.07	0.08	1.61	1.61	0.57	0.55	2.98	2.97	2	1.59	8	10.91	1.00
Alaskan duff core	0.08	0.09	1.64	1.63	-	-	-	-	-	-	-	-	-
Longleaf pine	0.10	0.11	1.77	1.80	0.61	0.57	2.45	2.45	1	1.55	10	96.01	0.92
Dry Douglas fir 2	0.07	0.07	1.64	1.67	0.47	0.45	2.78	2.71	1	1.61	9	12.63	1.01
Rice straw	0.08	0.08	1.59	1.60	0.20	0.20	2.12	2.09	2	1.41	10	382.7	0.92
LL Pine & wiregrass	0.10	0.10	1.66	1.65	0.46	0.46	2.60	2.57	2	1.54	10	84.92	0.91
Oak & hickory	0.07	0.10	1.70	1.65	-	-	-	-	-	-	-	-	-
Dry Douglas fir	0.08	0.09	1.68	1.66	0.44	0.43	2.76	2.74	2	1.57	9	12.98	1.00
Black needlerush 2	0.09	0.09	1.78	1.79	0.40	0.40	2.18	2.15	1	1.55	6	61.12	0.93
Black needlerush	0.13	0.14	1.75	1.72	0.55	0.52	2.40	2.35	1	1.55	9	195.44	0.87
White spruce	0.07	0.08	1.60	1.59	-	-	-	-	-	-	-	-	-
Rhododendron	0.07	0.08	1.61	1.61	-	-	-	-	-	-	-	-	-
Wiregrass	0.05	0.06	1.61	1.62	0.37	0.36	2.94	2.88	2	1.55	8	44.70	0.96
Sugarcane	0.07	0.07	1.56	1.57	-	-	-	-	-	-	-	-	-
Sagebrush	0.14	0.14	1.72	1.71	0.31	0.31	1.72	1.68	1	1.45	21	95.61	0.84
Miss. palmetto	0.09	0.10	1.65	1.65	-	-	-	-	-	-	-	-	-
Black spruce	0.08	0.09	1.86	1.79	-	-	-	-	-	-	-	-	-
Florida palmetto	0.08	0.09	1.66	1.72	-	-	-	-	-	-	-	-	-
Chamise	0.08	0.10	1.80	1.80	-	-	-	-	-	-	-	-	-
Gallberry	0.09	0.11	1.89	1.89	-	-	-	-	-	-	-	-	-
Fresh Douglas fir	0.07	0.09	1.72	1.73	-	-	-	-	-	-	-	-	-

[34] The uncertainty in the refractive index for LAC is due in part to the unknown void fraction which depends, among other things, on the combustion conditions [*Bond and Bergstrom*, 2006]. Higher void fractions lead to lower real and imaginary refractive indices as well as lower densities. We examined the effect of this uncertainty on refractive index and density calculated from composition by using the range in these variables suggested by *Bond and Bergstrom* [2006] in our calculations. This range in LAC properties is for fully graphitized EC with varying void fraction. *Schmid et al.* [2009] found that low temperature, smoldering combustion produced only partially graphitized EC, leading to a lower imaginary refractive index than used here. There is also considerable uncertainty in the properties we are assuming for OC. Although the values listed in Table 1 are commonly applied to OC aerosols, these are quantities which should be known better [*Schmid et al.*, 2009]. The refractive index and density values listed in Figures 2 and 3 are those calculated using the IMPROVE OC/EC split and the upper values for LAC density and refractive index listed in Table 1.

5. Size Distributions

[35] For FLAME 2 we calculated geometric mean diameters (D_g) and their standard deviations (σ_g) for each successfully aligned dry number (subscript n) and volume (subscript v) size distribution. *Hand et al.* [2002], using the same sizing and alignment technique used here, estimated uncertainties of 2% and 20% for these two parameters. The volume distributions were not completely captured by the DMPS, therefore volume mode statistics could only be calculated for burns where the OPC was not saturated and we were able to successfully align the OPC and DMPS data. Several fuels, including Alaskan duff core, wiregrass, dry Douglass fir and rice straw produced bimodal volume size distributions, while those for the smoke from the other fuels, for which we were able to compute volume distributions, were monomodal. All of the aligned number size distributions had only one discernible mode. The D_g and σ_g values were calculated for the entire distribution, even for the few multimodal cases.

[36] Table 2 lists the D_g and σ_g values for each FLAME 2 burn and indicates the number of modes for the aligned volume distributions. Geometric mean diameters for the number distributions generally moved toward larger values over the course of the experiment, with the rate of increase in D_{gn} decreasing as each experiment progressed. After one hour, the difference between consecutive D_{gn} values, 10 min apart, was less than 2% in all cases. The σ_{gn} values were much more constant, changing by less than 2% over the entire course of each experiment. The values listed in Table 2 show the first D_g and σ_g values measured for each burn as well as those measured one hour later, when the aerosol population had achieved a more steady distribution. The D_{gn} values measured after one hour ranged from 0.06–0.14 μm with the wiregrass burn producing the smallest D_{gn} and the sagebrush burn the largest. These values are consistent with those for fresh wildfire smoke presented by *Janhäll et al.* [2010].

[37] Comparing repeat burns with the same fuel, the D_{gn} values for the two black needlerush burns, measured after one hour, differed by 38%, while those for the two Alaskan duff core and dry Douglas fir burns both differed by about 21%. After one hour, σ_{gn} values ranged from 1.57–1.89 with sugarcane producing the smallest σ_{gn} value and gallberry the largest. Unlike D_{gn}, the σ_{gn} values for the duplicate fuels were quite similar, differing by about 4% for black needlerush burns and less than 1% for Alaskan duff core and dry Douglas fir burns.

[38] The D_{gv} values one hour after ignition ranged from 0.20–0.57 μm with smoke from the rice straw burn having the smallest value and longleaf pine the largest. One factor which could explain these large differences in volume distributions is combustion conditions, as more smoldering combustion has been shown to produce larger particles [*Reid et al.*, 2005b]. There is, however, very little difference in the MCE values for these burns, which would be expected for

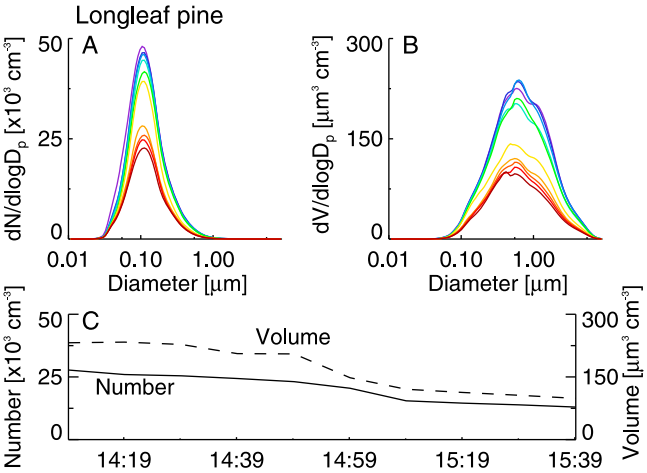

Figure 5. Aligned (a) number and (b) volume distributions from the FLAME 2 longleaf pine burn. Time progresses from purple to red with each distribution 10 min apart. (c) Integrated number (solid line) and volume (dashed line) concentrations for the same time period.

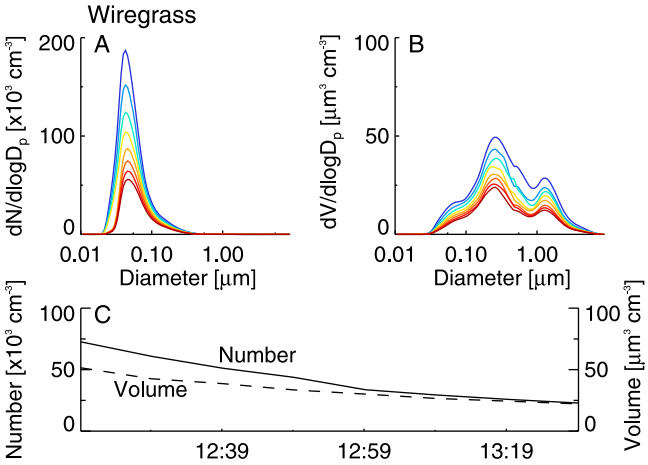

Figure 6. Similar to Figure 5 for the FLAME 2 wiregrass burn.

highly differing combustion conditions [*McMeeking et al.*, 2009]. It must be remembered that, unlike what may be the case in a field study, our measured MCE is a fire integrated value. Without other time resolved measurements we do not know how various combustion phases contributed to the total aerosol load and, thus, MCE may not be helpful in explaining the differences in burns seen here. During most experiments D_{gv} decreased over time; however, this decrease was less then the uncertainty in D_{gv} in every case.

[39] The sagebrush burn produced aerosols with the narrowest volume distribution, $\sigma_{gv} = 1.68$ while the Alaskan duff core 2 burn, one of the clearly bimodal cases, produced the widest, $\sigma_{gv} = 2.97$. This difference could also be due to combustion conditions as sagebrush burned with an intense flaming phase while Alaskan duff core only smoldered [*Reid et al.*, 2005b]. Again, however, the difference in the fire-integrated MCE values for these two burns is small. The σ_{gv} values for the two duplicate fuels for which we have volume distributions showed better agreement than the D_{gv} values. The D_{gv} values varied by 27% for the two black needlerush burns and 5% for the dry Douglas fir burns while σ_{gv} varied by 9% and 1% for burns of these two fuels respectively.

[40] Figures 5 and 6 show the evolution of number (Figures 5a and 6a) and volume (Figures 5b and 6b) distributions for two of the FLAME 2 burns, longleaf pine and wiregrass, as well as the integrated total number and volume concentrations (Figures 5c and 6c). Figure 7 shows the aligned volume distributions one hour after ignition.

6. Retrieved Effective Refractive Indices

[41] Table 2 also lists the effective refractive indices retrieved from the successful alignments ($m_{retrieved}$), as described in section 2.3, averaged over each experiment. This table also lists the slope and χ^2 value returned by the alignment and the number (N) of successfully aligned distributions for each burn. The $m_{retrieved}$ values remained fairly constant over the course of each experiment, changing by less than 2% in all cases. This consistency in $m_{retrieved}$ likely indicates that aerosol composition and shape, at least in the overlap region between the DMPS and OPC measurements, also remained constant over the course of each experiment. Experiment-averaged $m_{retrieved}$ values ranged from 1.41 to 1.61 with the rice straw having the lowest and the dry Douglas fir 2 burn the highest values.

[42] The differences between the retrieved effective refractive indices for the two duplicate fuel burns for which

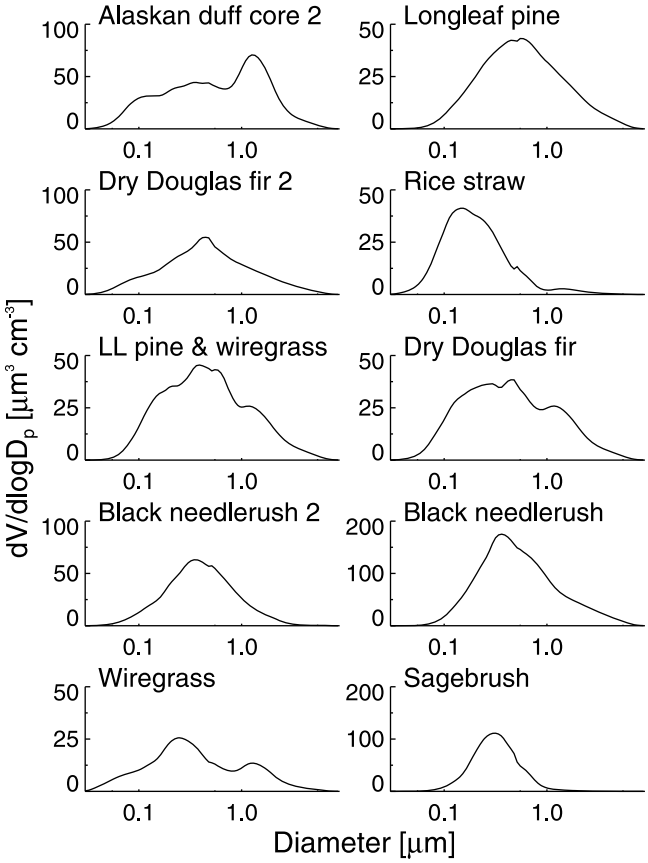

Figure 7. Aligned volume distributions for specified FLAME 2 burns one hour after ignition.

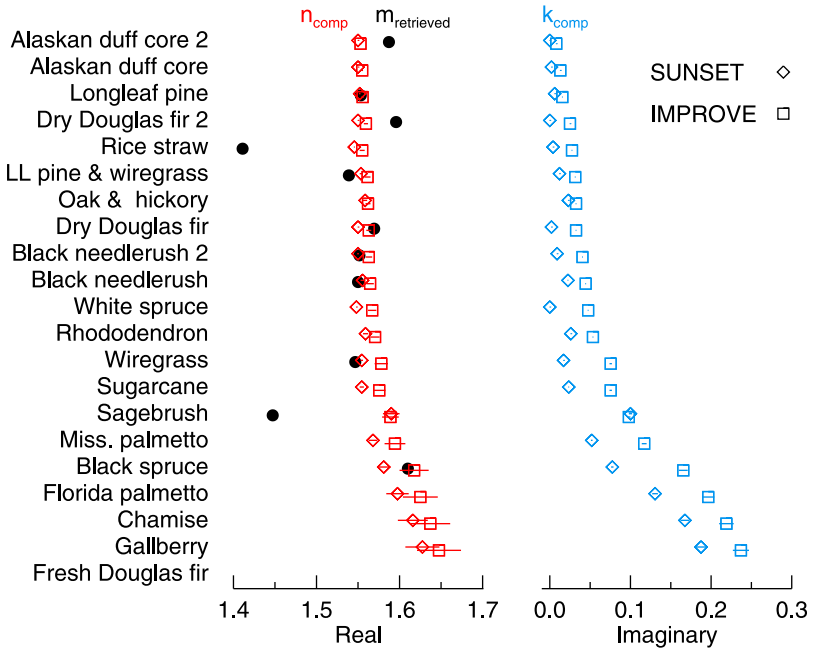

Figure 8. FLAME 2 alignment retrieved effective refractive index (black) and real (red) and imaginary (blue) refractive indices calculated from $PM_{2.5}$ composition data. Diamonds indicate values calculated using the Sunset organic carbon/elemental carbon (OC/EC) split and squares those calculated using the IMPROVE OC/EC split. Lines indicate the range in calculated values due to the different LAC assumptions (Table 1). Burns are ranked from least to most light absorbing.

we were able to retrieve values were less than 2% in both cases. The dry Douglas fir burn produced aerosols with $m_{retrieved}$ = 1.57 while the dry Douglas fir burn 2 had $m_{retrieved}$ = 1.61. The two black needlerush burns both had average $m_{retrieved}$ values of 1.55.

[43] Figure 8 shows the average $m_{retrieved}$ (black) values for each burn from FLAME 2 as well as the n_{comp} (red) and k_{comp} (blue) values (section 4). Burns are ranked in the same order as Figure 3. The squares show values calculated using the IMPROVE OC/EC split and the diamonds those using the Sunset OC/EC split. The uncertainty bars in Figure 8 represent the range in values due to the different assumed LAC properties. As can be seen, the agreement between the retrieved effective refractive index and n_{comp} is good, within 2%, for every case except rice straw and sagebrush. Rice straw was unique in that it was the only fuel which produced aerosols with a high inorganic mass fraction but a very low LAC mass fraction. Thus, this discrepancy could indicate a problem with some of our assumptions about the form or properties of the inorganic salts in this case. Sagebrush produced more absorbing aerosols, hence higher k_{comp}. The discrepancy between the refractive indices in this case highlights the problems associated with the OPC sizing technique for strongly light absorbing particles, as described above.

[44] Both the retrieved effective refractive indices and calculated complex refractive indices are similar to other values for biomass burning aerosols reported in the literature. *McMeeking et al.* [2005a] reported effective refractive index values of 1.56–1.59 (λ = 632.8 nm) during smoke influenced periods at Yosemite National Park, USA using the same sizing and alignment method used here. *Hungershoefer et al.* [2008] measured values of 1.60 + i0.01 and 1.56 + i0.01 (λ = 550 nm) for fresh smoke from two different fuels burned during a similar laboratory experiment and also reported a possible range of 1.41 to 1.60 for real refractive index and 0.0093 to 0.1 for the imaginary part of the refractive index for biomass burning emissions.

7. Dry Mass Scattering Efficiency

[45] We used Mie theory and the various FLAME 2 retrieved effective and calculated complex refractive index values to calculate dry scattering efficiency (Q_{scat}) as a function of particle size at a wavelength of 532 nm (to match the PAS and interpolated nephelometer values). We then used these values to calculate scattering coefficients (b_{sp}) from the binned aerosol number concentrations (N_i), where i is bin number, using [*Seinfeld and Pandis*, 2006]:

$$b_{sp} = \sum_i \frac{\pi D_{p,i}^2}{4} N_i Q_{scat,i} \quad (4)$$

[46] After calculating b_{sp}, we used these values as well as total mass concentrations (M) calculated from volume distributions (shown in Figure 8) and ρ_{comp} to calculate dry mass scattering efficiencies (*MSE*):

$$\mathrm{MSE} = \frac{b_{sp}}{M} \quad (5)$$

In the calculations, both retrieved effective refractive indices and those computed from chemical composition data were used; we denote the corresponding *MSE* as $MSE_{retrieved}$ and MSE_{comp}. We also calculated MSE using b_{sp} measured

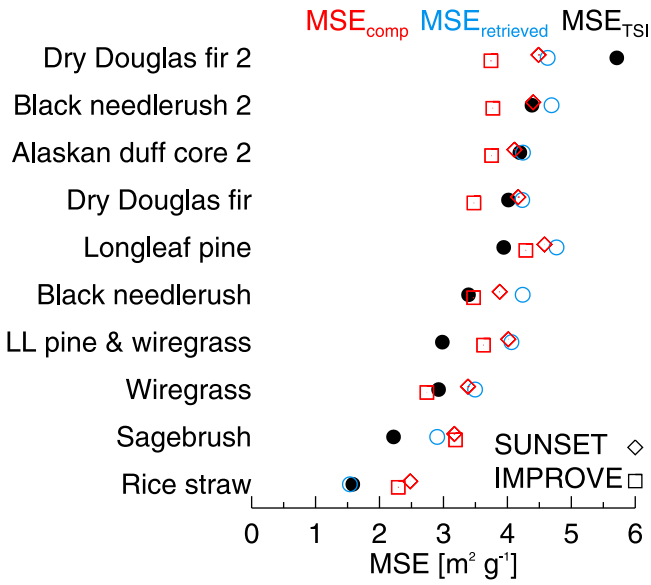

Figure 9. Mass scattering efficiency *MSE* [m^2 g^{-1}] at 532 nm calculated using measured scattering (black) and scattering calculated from retrieved (blue) and composition (red) refractive indices. Symbol shape has the same meaning as in Figure 8.

by the TSI nephelometer and the same *M* values as above and denote this as MSE_{TSI}.

[47] Figure 9 shows the burns ranked by MSE_{TSI} (black circles). Again, only cases where the alignment was successful are shown. Values ranged from 1.5–5.7 m^2 g^{-1} with the majority of the values between 2.0 and 4.5 m^2 g^{-1}. Aerosols from the dry Douglas fir 2 burn had the highest MSE_{TSI} value and those from the rice straw burn the lowest. *Reid et al.* [2005a] report a typical *MSE* range of 2.8–4.2 for fresh smoke characterized during various field studies. The larger range in *MSE* that we calculated from FLAME 2 data may result from the wide range of fuel types individually burned during the study and the freshness of the emissions at the time of the measurements.

[48] Figure 9 also shows the *MSE* values calculated using retrieved effective refractive indices ($MSE_{retrieved}$) and those calculated from composition (MSE_{comp}). As with the refractive indices, four values of MSE_{comp} were calculated, using the IMPROVE and Sunset OC/EC splits and the extremes of LAC properties shown in Table 1. The differences in OC/EC splits caused significant differences in MSE_{comp}. However, the effects of changing the LAC properties were negligible. All of the different estimates of MSE trend together; however, there are some discrepancies in the different values. For MSE_{comp}, the higher values tend to be lower than MSE_{TSI} while those at the low end are higher. Using the Sunset OC/EC split provides better agreement for the higher values; however it increases the discrepancies at the low end. In general, $MSE_{retrieved}$ provides a better estimate of MSE_{TSI} than MSE_{comp}. This implies that although, as noted above, $m_{retrieved}$ may not accurately represent the real refractive index, especially for absorbing aerosols, this effective refractive index can be used to reconstruct scattering, as it is essentially derived from a scattering measurement (the OPC).

[49] Figure 10a shows the correlations between MSE_{TSI} and D_{gv}. These variables are somewhat correlated with an R^2 value of 0.57 and a slope of 7.33. Many other studies have shown that *MSE* is strongly correlated with aerosol size distribution [*Hand and Malm*, 2007; *McMeeking et al.*, 2005a; *Pitchford et al.*, 2007]. Calculated MSE_{TSI} values were more strongly correlated with $m_{retrieved}$ with an R^2 value of 0.83 and a slope of 17.73 (Figure 10b). This is also expected as a higher effective refractive index indicates more scattering, for equivalent particle sizes.

8. Dry Mass Absorption Efficiency

[50] Similar to the approach for *MSE*, we calculated values of dry mass absorption efficiency (*MAE*) at 532 nm:

$$\mathrm{MAE} = \frac{b_{ap}}{M} \tag{6}$$

Absorption coefficients (b_{ap}) measured directly by the PAS were used, with the total mass concentration *M* computed as discussed above, to generate MAE_{PAS}. We also computed values of MAE_{comp} using the same aerosol size distributions, densities, and refractive indices as used for the MSE_{comp} calculations. Figure 11 shows the burns ranked by MAE_{PAS} from highest to lowest. All the values fall between 0 and 1 m^2 g^{-1}, with sagebrush having the highest value, 0.94 m^2 g^{-1}, and Alaskan duff core the lowest, 0.04 m^2 g^{-1}. *Hungershoefer et al.* [2008] reported MAE values of

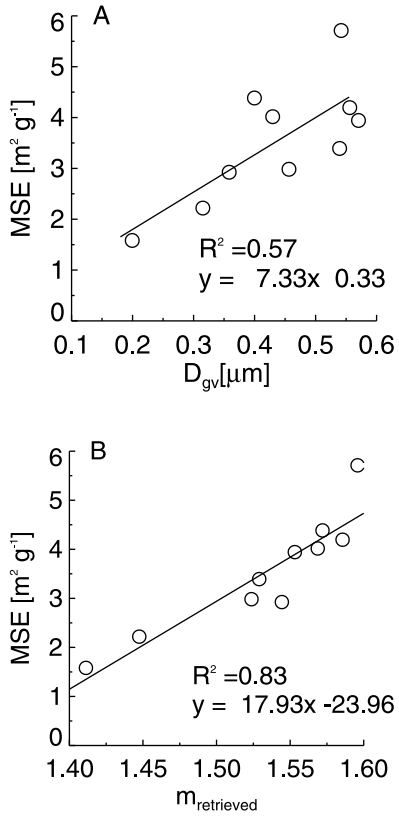

Figure 10. Mass scattering efficiency *MSE* [m^2 g^{-1}] at 532 nm calculated from measured scattering versus (a) D_{gv} [μm] and (b) $m_{retrieved}$. Solid lines are regression lines.

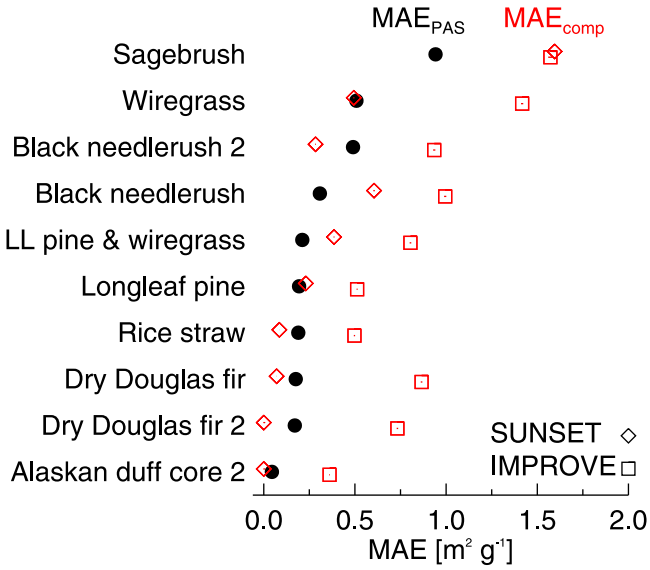

Figure 11. Mass absorbing efficiency *MAE* [m^2 g^{-1}] at 532 nm calculated using measured absorption (black) and absorption calculated from composition (red) refractive indices. Symbol shape has the same meaning as in Figure 8.

0.51 ± 0.02 m^2 g^{-1} and 0.50 ± 0.02 m^2 g^{-1} for laboratory combustion of African grasses and hardwoods. *Reid et al.* [2005a] compiled a list of *MAE* values reported for aged regional smokes which ranged from 0.45 m^2 g^{-1} to 1.1 m^2 g^{-1}. The range in values from the FLAME 2 data is again somewhat larger than those in the literature, likely for the same reasons as stated above. Figure 11 also shows the MAE_{comp} values calculated using the various LAC assumptions. Again, changing the assumed refractive index and density of LAC had a minimal effect on MAE_{comp}. Changing the OC/EC split, however, proved to be very important, with the Sunset values producing better agreement between MAE_{comp} and MAE_{PAS} for all but the sagebrush burn.

[51] Figure 12 shows the relationships between MAE_{PAS} and d_{gv} (Figure 12a) $m_{retrieved}$ (Figure 12b) and k_{comp} (Figure 12c). Unlike MSE_{TSI}, which was positively correlated with both d_{gv} and $m_{retrieved}$, MAE_{PAS} is only weakly anti-correlated with both variables. This is to be expected as small particles (i.e., in the Rayleigh regime) are volume absorbers and *MAE* is independent of particle size [*Moosmüller and Arnott*, 2009]. For somewhat larger particles, *MAE* starts to decrease as a function of particle diameter as the light cannot fully penetrate the particle [*Moosmüller and Arnott*, 2009; *Moosmüller et al.*, 2009]. There is, however, a strong positive correlation between MAE_{PAS} and k_{comp} with an R^2 value of 0.88 and a slope of 8.76, because bulk absorption is proportional to k, which has a strong effect on particle absorption [*Moosmüller et al.*, 2009].

9. Conclusions

[52] Biomass burning emissions are a major contributor to the global aerosol burden and have important impacts on visibility degradation and radiative balance. However, there is still much uncertainty about many of the properties of these particles. The aerosol physical, chemical, and optical property data presented here for emissions from the combustion of various biomass fuels demonstrate large fuel-to-fuel and combustion-phase variations in the radiative properties of aerosol emissions from biomass burning. We expect characteristics such as the aerosol size distribution to evolve in the atmosphere after emission, dilution, and transport, and indeed even the size distributions from replicate burns differed in our studies. In contrast, although aerosol chemical composition, as derived from filter data, varied significantly between fuels, it was quite similar for replicate burns of the same fuels, even across both FLAME studies and with varying ignition techniques. Almost all of the fuels produced highly carbon dominated aerosols, with OM accounting for the largest mass

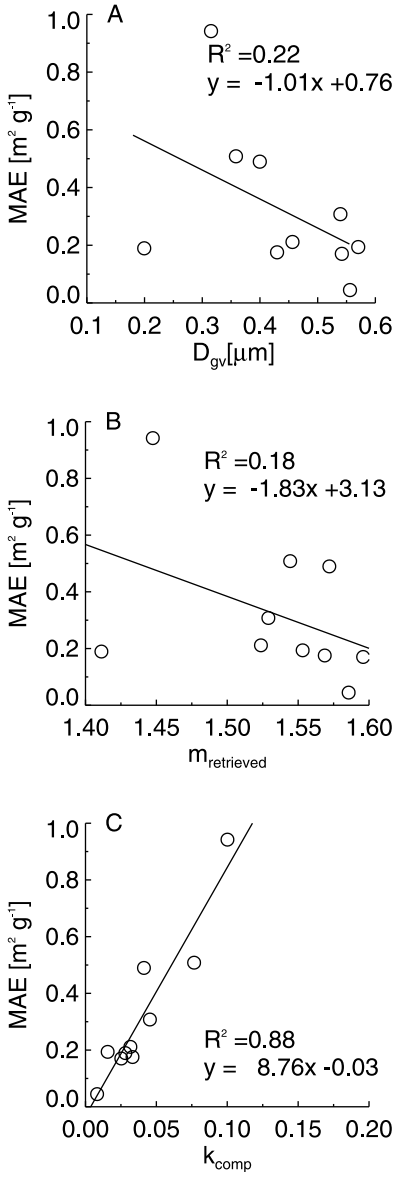

Figure 12. Mass absorption efficiency *MAE* [m^2 g^{-1}] at 532 nm calculated from measured absorption versus (a) D_{gv} [μm], (b) $m_{retrieved}$ and (c) k_{comp}. Solid lines are regression lines.

fraction in most cases, although many fuels also produced large quantities of EC. The variation in EC (assumed to be equal to LAC) mass fraction is especially important for determining radiative effects, as LAC is the most important light absorbing component of atmospheric aerosols. A few fuels, such as rice straw and palmetto, produced aerosols with inorganic mass fractions close to 0.5. These aerosols are likely to be much more hygroscopic than those with smaller fractions of inorganic species and thus could have enhanced effects on visibility reduction due to water uptake [*Carrico et al.*, 2008; *Carrico et al.*, 2010], as well as readily serving as cloud condensation nuclei in the atmosphere [*Petters et al.*, 2009a; *Petters et al.*, 2009b].

[53] We used the bulk composition data to calculate aerosol density and refractive index and found a large range in our data set, with computed density values from 1.22–1.89 g cm^{-3}, and real and imaginary refractive indices (at visible wavelengths) ranging from 1.55–1.80 and 0.01–0.50, respectively. Adding to this already large range in biomass burning aerosol properties is the inherent uncertainty in both the mass fraction of measured EC and the density and complex refractive index assumed for LAC. Applying the OC/EC splits determined by two different analytical techniques in our calculations changed the optical properties significantly, with the data from the Sunset instruments generally in better agreement with our direct optical data.

[54] Effective refractive indices retrieved from the alignment ($m_{retrieved}$) of DMA and OPC data also had a large range across different experiments, with values ranging from 1.41 to 1.61. However, retrieved effective refractive indices remained nearly constant over the course of each burn, changing by less than 2%, and replicate fuel experiments showed agreement also within 2%. Further, the retrieved effective refractive indices led to computed estimates of mass scattering efficiencies (MSE) that agreed well with our more direct measurements, even for those cases where there was a discrepancy between the effective refractive indices and real refractive indices calculated from composition. We thus propose that these effective refractive indices, along with size distributions, can be used to model the optical properties of particles produced from the combustion of our tested fuels, for similar fire-integrated MCE, since emissions are known to be sensitive to this parameter [*McMeeking et al.*, 2009].

[55] Dry mass absorbing efficiencies at 532 nm, calculated using b_{ap} measured by the PAS, ranged between 0.04 and 0.94 $m^2\ g^{-1}$, and were relatively independent of particle size but strongly correlated with k_{comp}, which in turn was highly dependent on the fuel burned. We also found that the OC/EC split had a much larger effect on MAE_{comp} values than did the different assumed LAC refractive index and density values. However, light absorption by aerosol organic carbon species present in biomass burning emissions was not explicitly considered here. Its impact on total aerosol absorption may be substantial, particularly at shorter wavelengths, and models of the spectral variation of biomass burning aerosol optical properties should include effects from absorbing OC [*Chakrabarty et al.*, 2009; *Schmid et al.*, 2009].

[56] **Acknowledgments.** A number of people were instrumental in the success of the FLAME studies. We would like to especially acknowledge the staff at the Fire Sciences Laboratory for their assistance. We thank Charles McDade and Lowell Ashbaugh at the Crocker Nuclear Laboratory, University of California, Davis, for providing the IMPROVE samplers and chemical analysis. Funding for this project was provided by the National Park Service and by the Joint Fire Science Program under Project JFSP 05-3-1-06. GRM acknowledges the support of a Department of Energy Global Change Education Program Graduate Research Environmental Fellowship.

References

Abel, S. J., J. M. Haywood, E. J. Highwood, J. Li, and P. R. Buseck (2003), Evolution of biomass burning aerosol properties from an agricultural fire in southern Africa, *Geophys. Res. Lett.*, *30*(15), 1783, doi:10.1029/2003GL017342.

Anderson, T. L., and J. A. Ogren (1998), Determining aerosol radiative properties using the TSI 3563 integrating nephelometer, *Aerosol Sci. Technol.*, *29*(1), 57–69, doi:10.1080/02786829808965551.

Anderson, T. L., et al. (1996), Performance characteristics of a high-sensitivity, three-wavelength, total scatter/backscatter nephelometer, *J. Atmos. Oceanic Technol.*, *13*(5), 967–986, doi:10.1175/1520-0426(1996)013<0967:PCOAHS>2.0.CO;2.

Andreae, M. O., et al. (1998), Airborne studies of aerosol emissions from savanna fires in southern Africa: 2. Aerosol chemical composition, *J. Geophys. Res.*, *103*(D24), 32,119–32,128, doi:10.1029/98JD02280.

Arnott, W. P., H. Moosmüller, C. F. Rogers, T. F. Jin, and R. Bruch (1999), Photoacoustic spectrometer for measuring light absorption by aerosol: Instrument description, *Atmos. Environ.*, *33*(17), 2845–2852, doi:10.1016/S1352-2310(98)00361-6.

Arnott, W. P., H. Moosmüller, and J. W. Walker (2000), Nitrogen dioxide and kerosene-flame soot calibration of photoacoustic instruments for measurement of light absorption by aerosols, *Rev. Sci. Instrum.*, *71*(12), 4545–4552, doi:10.1063/1.1322585.

Bae, M. S., J. J. Schauer, J. T. DeMinter, J. R. Turner, D. Smith, and R. A. Cary (2004), Validation of a semi-continuous instrument for elemental carbon and organic carbon using a thermal-optical method, *Atmos. Environ.*, *38*(18), 2885–2893, doi:10.1016/j.atmosenv.2004.02.027.

Bäumer, D., U. Lohmann, G. Lesins, J. Li, and B. Croft (2007), Parameterizing the optical properties of carbonaceous aerosols in the Canadian Centre for Climate Modeling and Analysis Atmospheric General Circulation Model with impacts on global radiation and energy fluxes, *J. Geophys. Res.*, *112*, D10207, doi:10.1029/2006JD007319.

Bond, T. C., and R. W. Bergstrom (2006), Light absorption by carbonaceous particles: An investigative review, *Aerosol Sci. Technol.*, *40*(1), 27–67, doi:10.1080/02786820500421521.

Bond, T. C., D. S. Covert, and T. Muller (2009), Truncation and angular-scattering corrections for absorbing aerosol in the TSI 3563 nephelometer, *Aerosol Sci. Technol.*, *43*(9), 866–871, doi:10.1080/02786820902998373.

Boparai, P., J. M. Lee, and T. C. Bond (2008), Revisiting thermal-optical analyses of carbonaceous aerosol using a physical model, *Aerosol Sci. Technol.*, *42*(11), 930–948, doi:10.1080/02786820802360690.

Carrico, C. M., M. D. Petters, S. M. Kreidenweis, J. L. Collett, G. Engling, and W. C. Malm (2008), Aerosol hygroscopicity and cloud droplet activation of extracts of filters from biomass burning experiments, *J. Geophys. Res.*, *113*, D08206, doi:10.1029/2007JD009274.

Carrico, C. M., M. D. Petters, S. M. Kreidenweis, G. R. McMeeking, E. J. T. Levin, W. C. Malm, J. Jeffrey, and L. Collett (2010), Water uptake and chemical composition of fresh aerosols generated in open burning of biomass, *Atmos. Chem. Phys. Discuss.*, *10*, 3627–3658, doi:10.5194/acpd-10-3627-2010.

Chakrabarty, R. K., H. Moosmüller, M. A. Garro, W. P. Arnott, J. Walker, R. A. Susott, R. E. Babbitt, C. E. Wold, E. N. Lincoln, and W. M. Hao (2006), Emissions from the laboratory combustion of wildland fuels: Particle morphology and size, *J. Geophys. Res.*, *111*, D07204, doi:10.1029/2005JD006659.

Chakrabarty, R. K., H. Moosmüller, W. P. Arnott, M. A. Garro, J. G. Slowik, E. S. Cross, J. H. Han, P. Davidovits, T. B. Onasch, and D. R. Worsnop (2007), Light scattering and absorption by fractal-like carbonaceous chain aggregates: Comparison of theories and experiment, *Appl. Opt.*, *46*, 6990–7006, doi:10.1364/AO.46.006990.

Chakrabarty, R. K., H. Moosmüller, L.-W. A. Chen, K. Lewis, W. P. Arnott, C. Mazzoleni, M. K. Dubey, C. E. Wold, W. M. Hao, and S. M. Kreidenweis (2009), Brown carbon in tar balls from smoldering biomass combustion, *Atmos. Chem. Phys.*, *10*, 6363–6370, doi:10.5194/acp-10-6363-2010.

Chen, L. W. A., H. Moosmüller, W. P. Arnott, J. C. Chow, J. G. Watson, R. A. Susott, R. E. Babbitt, C. E. Wold, E. N. Lincoln, and W. M. Hao (2007), Emissions from laboratory combustion of wildland fuels: Emis-

sion factors and source profiles, *Environ. Sci. Technol.*, *41*(12), 4317–4325, doi:10.1021/es062364i.

Chow, J. C., J. G. Watson, L. W. A. Chen, M. C. O. Chang, N. F. Robinson, D. Trimble, and S. Kohl (2007), The IMPROVE-A temperature protocol for thermal/optical carbon analysis: Maintaining consistency with a long-term database, *J. Air Waste Manage. Assoc.*, *57*(9), 1014–1023, doi:10.3155/1047-3289.57.9.1014.

Christian, T. J., R. J. Yokelson, J. A. Carvalho, D. W. T. Griffith, E. C. Alvarado, J. C. Santos, T. G. S. Neto, C. A. G. Veras, and W. M. Hao (2007), The tropical forest and fire emissions experiment: Trace gases emitted by smoldering logs and dung from deforestation and pasture fires in Brazil, *J. Geophys. Res.*, *112*, D18308, doi:10.1029/2006JD008147.

DeBell, L. J., K. A. Gebhart, J. L. Hand, W. C. Malm, M. L. Pitchford, B. A. Schichtel, and W. H. White (2006), *Spatial and seasonal patterns and temporal variability of haze and its constituents in the United States*, *Rep. 4*, Coop. Inst. for Res. in the Atmos., Fort Collins, Colo.

DeCarlo, P. F., J. G. Slowik, D. R. Worsnop, P. Davidovits, and J. L. Jimenez (2004), Particle morphology and density characterization by combined mobility and aerodynamic diameter measurements. Part 1: Theory, *Aerosol Sci. Technol.*, *38*(12), 1185–1205, doi:10.1080/027868290903907.

Formenti, P., W. Elbert, W. Maenhaut, J. Haywood, S. Osborne, and M. O. Andreae (2003), Inorganic and carbonaceous aerosols during the Southern African Regional Science Initiative (SAFARI 2000) experiment: Chemical characteristics, physical properties, and emission data for smoke from African biomass burning, *J. Geophys. Res.*, *108*(D13), 8488, doi:10.1029/2002JD002408.

Freney, E. J., S. T. Martin, and P. R. Buseck (2009), Deliquescence and efflorescence of potassium salts relevant to biomass-burning aerosol particles, *Aerosol Sci. Technol.*, *43*(8), 799–807, doi:10.1080/02786820902946620.

Hand, J. L. (2001), *A new technique for obtaining aerosol size distributions with applications to estimates of aerosol properties*, Ph.D. dissertation, Colo. State Univ., Fort Collins.

Hand, J. L., and S. M. Kreidenweis (2002), A new method for retrieving particle refractive index and effective density from aerosol size distribution data, *Aerosol Sci. Technol.*, *36*(10), 1012–1026, doi:10.1080/02786820290092276.

Hand, J. L., and W. C. Malm (2007), Review of aerosol mass scattering efficiencies from ground-based measurements since 1990, *J. Geophys. Res.*, *112*, D16203, doi:10.1029/2007JD008484.

Hand, J. L., S. M. Kreidenweis, D. E. Sherman, J. L. Collett, S. V. Hering, D. E. Day, and W. C. Malm (2002), Aerosol size distributions and visibility estimates during the Big Bend regional aerosol and visibility observational (BRAVO) study, *Atmos. Environ.*, *36*(32), 5043–5055, doi:10.1016/S1352-2310(02)00568-X.

Hasan, H., and T. G. Dzubay (1983), Apportioning light extinction coefficients to chemical-species in atmospheric aerosol, *Atmos. Environ.*, *17*(8), 1573–1581, doi:10.1016/0004-6981(83)90310-4.

Hodzic, A., S. Madronich, B. Bohn, S. Massie, L. Menut, and C. Wiedinmyer (2007), Wildfire particulate matter in Europe during summer 2003: Meso-scale modeling of smoke emissions, transport and radiative effects, *Atmos. Chem. Phys.*, *7*, 4043–4064, doi:10.5194/acp-7-4043-2007.

Hungershoefer, K., K. Zeromskiene, Y. H. Iinuma, G. Helas, J. Trentmann, T. Trautmann, R. S. Parmar, A. Wiedensohler, M. O. Andreae, and O. Schmid (2008), Modeling the optical properties of fresh biomass burning aerosol produced in a smoke chamber: Results from the EFEU campaign, *Atmos. Chem. Phys.*, *8*, 3427–3439, doi:10.5194/acp-8-3427-2008.

Janhäll, S., M. O. Andreae, and U. Poschl (2010), Biomass burning aerosol emissions from vegetation fires: Particle number and mass emission factors and size distributions, *Atmos. Chem. Phys.*, *10*, 1427–1439, doi:10.5194/acp-10-1427-2010.

Kasischke, E. S., and J. E. Penner (2004), Improving global estimates of atmospheric emissions from biomass burning, *J. Geophys. Res.*, *109*, D14S01, doi:10.1029/2004JD004972.

Levin, E. J. T., S. M. Kreidenweis, G. R. McMeeking, C. M. Carrico, J. L. Collett, and W. C. Malm (2009), Aerosol physical, chemical and optical properties during the Rocky Mountain Airborne Nitrogen and Sulfur study, *Atmos. Environ.*, *43*(11), 1932–1939, doi:10.1016/j.atmosenv.2008.12.042.

Lide, D. R. (Ed.) (2008), *CRC Handbook of Chemistry and Physics*, CRC, Boca Raton, Fla.

Liu, L., M. I. Mishchenko, and W. P. Arnott (2008), A study of radiative properties of fractal soot aggregates using the superposition T-matrix method, *J. Quant. Spectrosc. Radiat. Transfer*, *109*, 2656–2663, doi:10.1016/j.jqsrt.2008.05.001.

Mack, L. E. (2008), Cavity ring-down spectroscopy and the retrieval of optical properties of aerosols produced by biomass burning during FLAME 2, M.S. thesis, Colo. State Univ., Fort Collins.

Mack, L., et al. (2010), Optical closure experiments for biomass smoke aerosols, *Atmos. Chem. Phys. Discuss.*, *10*, 7469–7494, doi:10.5194/acpd-10-7469-2010.

Malm, W. C., and J. L. Hand (2007), An examination of the physical and optical properties of aerosols collected in the IMPROVE program, *Atmos. Environ.*, *41*(16), 3407–3427, doi:10.1016/j.atmosenv.2006.12.012.

Malm, W. C., J. F. Sisler, D. Huffman, R. A. Eldred, and T. A. Cahill (1994), Spatial and seasonal trends in particle concentrations and optical extinction in the United States, *J. Geophys. Res.*, *99*(D1), 1347–1370, doi:10.1029/93JD02916.

Martins, J. V., P. V. Hobbs, R. E. Weiss, and P. Artaxo (1998), Sphericity and morphology of smoke particles from biomass burning in Brazil, *J. Geophys. Res.*, *103*(D24), 32,051–32,057, doi:10.1029/98JD01153.

McMeeking, G. R., S. M. Kreidenweis, C. M. Carrico, J. L. Collett, D. E. Day, and W. C. Malm (2005a), Observations of smoke-influenced aerosol during the Yosemite Aerosol Characterization Study: 2. Aerosol scattering and absorbing properties, *J. Geophys. Res.*, *110*, D18209, doi:10.1029/2004JD005624.

McMeeking, G. R., S. M. Kreidenweis, C. M. Carrico, T. Lee, J. L. Collett, and W. C. Malm (2005b), Observations of smoke-influenced aerosol during the Yosemite Aerosol Characterization Study: Size distributions and chemical composition, *J. Geophys. Res.*, *110*, D09206, doi:10.1029/2004JD005389.

McMeeking, G. R., et al. (2006), Smoke-impacted regional haze in California during the summer of 2002, *Agric. For. Meteorol.*, *137*(1–2), 25–42, doi:10.1016/j.agrformet.2006.01.011.

McMeeking, G. R., et al. (2009), Emissions of trace gases and aerosols during the open combustion of biomass in the laboratory, *J. Geophys. Res.*, *114*, D19210, doi:10.1029/2009JD011836.

Moosmüller, H., and W. P. Arnott (2003), Angular truncation errors in integrating nephelometry, *Rev. Sci. Instrum.*, *74*(7), 3492–3501, doi:10.1063/1.1581355.

Moosmüller, H., and W. P. Arnott (2009), Particle optics in the Rayleigh regime, *J. Air Waste Manage.*, *59*(9), 1028–1031, doi:10.3155/1047-3289.59.9.1028.

Moosmüller, H., R. K. Chakrabarty, and W. P. Arnott (2009), Aerosol light absorption and its measurement: A review, *J. Quant. Spectrosc. Radiat. Transfer*, *110*, 844–878, doi:10.1016/j.jqsrt.2009.02.035.

Novakov, T., and C. E. Corrigan (1995), Thermal characterization of biomass smoke particles, *Mikrochim. Acta*, *119*(1–2), 157–166, doi:10.1007/BF01244864.

Park, R. J., D. J. Jacob, and J. A. Logan (2007), Fire and biofuel contributions to annual mean aerosol mass concentrations in the United States, *Atmos. Environ.*, *41*(35), 7389–7400, doi:10.1016/j.atmosenv.2007.05.061.

Petters, M. D., C. M. Carrico, S. M. Kreidenweis, A. J. Prenni, P. J. DeMott, J. L. Collett, and H. Moosmüller (2009a), Cloud condensation nucleation activity of biomass burning aerosol, *J. Geophys. Res.*, *114*, D22205, doi:10.1029/2009JD012353.

Petters, M. D., et al. (2009b), Ice nuclei emissions from biomass burning, *J. Geophys. Res.*, *114*, D07209, doi:10.1029/2008JD011532.

Pitchford, M., W. Malm, B. Schichtel, N. Kumar, D. Lowenthal, and J. Hand (2007), Revised algorithm for estimating light extinction from IMPROVE particle speciation data, *J. Air Waste Manage. Assoc.*, *57*(11), 1326–1336, doi:10.3155/1047-3289.57.11.1326.

Reid, J. S., T. F. Eck, S. A. Christopher, R. Koppmann, O. Dubovik, D. P. Eleuterio, B. N. Holben, E. A. Reid, and J. Zhang (2005a), A review of biomass burning emissions part III: Intensive optical properties of biomass burning particles, *Atmos. Chem. Phys.*, *5*, 827–849, doi:10.5194/acp-5-827-2005.

Reid, J. S., R. Koppmann, T. F. Eck, and D. P. Eleuterio (2005b), A review of biomass burning emissions part II: Intensive physical properties of biomass burning particles, *Atmos. Chem. Phys.*, *5*, 799–825, doi:10.5194/acp-5-799-2005.

Schmid, O., D. Chand, E. Karg, P. Guyon, G. P. Frank, E. Swietlicki, and M. O. Andreae (2009), Derivation of the density and refractive index of organic matter and elemental carbon from closure between physical and chemical aerosol properties, *Environ. Sci. Technol.*, *43*(4), 1166–1172, doi:10.1021/es800570p.

Seinfeld, J. H., and S. N. Pandis (2006), *Atmospheric Chemistry and Physics: From Air Pollution to Climate Change*, 2nd ed., 1203 pp., John Wiley, Hoboken, N. J.

Slowik, J. G., K. Stainken, P. Davidovits, L. R. Williams, J. T. Jayne, C. E. Kolb, D. R. Worsnop, Y. Rudich, P. F. DeCarlo, and J. L. Jimenez (2004), Particle morphology and density characterization by combined

mobility and aerodynamic diameter measurements. Part 2: Application to combustion-generated soot aerosols as a function of fuel equivalence ratio, *Aerosol Sci. Technol.*, *38*(12), 1206–1222, doi:10.1080/027868290903916.

Tang, I. N. (1996), Chemical and size effects of hygroscopic aerosols on light scattering coefficients, *J. Geophys. Res.*, *101*(D14), 19,245–19,250, doi:10.1029/96JD03003.

Turpin, B. J., and H. J. Lim (2001), Species contributions to PM2.5 mass concentrations: Revisiting common assumptions for estimating organic mass, *Aerosol Sci. Technol.*, *35*(1), 602–610, doi:10.1080/02786820152051454.

Watson, J. G. (2002), Visibility: Science and regulation, *J. Air Waste Manage. Assoc.*, *52*(6), 628–713.

Watson, J. G., J. C. Chow, and L. W. A. Chen (2005), Summary of organic and elemental carbon/black carbon analysis methods and intercomparisons, *Aerosol Air Quality Res.*, *5*(1), 65–102.

Yokelson, R. J., et al. (2009), Emissions from biomass burning in the Yucatan, *Atmos. Chem. Phys.*, *9*, 5785–5812, doi:10.5194/acp-9-5785-2009.

W. P. Arnott and H. Moosmüller, Division of Atmospheric Sciences, Desert Research Institute, Reno, NV 89512, USA.

C. M. Carrico, J. L. Collett Jr., S. M. Kreidenweis, E. J. T. Levin, and L. E. Mack, Department of Atmospheric Science, Colorado State University, Fort Collins, CO 80523, USA. (eleven@atmos.colostate.edu)

W. M. Hao and E. Wold, Fire Sciences Laboratory, Rocky Mountain Research Station, USDA Forest Service, Missoula, MT 59808, USA.

W. C. Malm, U.S. National Park Service, Cooperative Institute for Research in the Atmosphere, Colorado State University, Fort Collins, CO 80523, USA.

G. R. McMeeking, Centre for Atmospheric Science, University of Manchester, Manchester M13 9PL, UK.